Contents lists available at ScienceDirect

Journal of King Saud University – Science

Original article

DFT and molecular docking study of chloroquine derivatives as antiviral to coronavirus COVID-19

Olfa Noureddine [a], Noureddine Issaoui [a],*, Omar Al-Dossary [b],*

[a] University of Monastir, Laboratory of Quantum and Statistical Physics (LR18ES18), Faculty of Sciences, Monastir 5079, Tunisia
[b] Department of Physics and Astronomy, College of Science, King Saud University, PO Box 2455, Riyadh 11451, Saudi Arabia

ARTICLE INFO

ABSTRACT

The recently emerged COVID-19 virus caused hundreds of thousands of deaths and instigated a widespread fear, threatening the world's most advanced health security. In 2020, chloroquine derivatives are among the drugs tested against the coronavirus pandemic and showed an apparent efficacy. In the present work, the chloroquine and the chloroquine phosphate molecules have been proposed as potential antiviral for the treatment of COVID-19 diseases combining DFT and molecular docking calculations. Molecular geometries, electronic properties and molecular electrostatic potential were investigated using density functional theory (DFT) at the B3LYP/6-31G* method. As results, we found a good agreement between the theoretical and the experimental geometrical parameters (bond lengths and bond angles). The frontier orbitals analysis has been calculated at the same level of theory to determine the charge transfer within the molecule. In order to perform a better description of the FMOs, the density of states was determined. The molecular electrostatic potential maps were calculated to provide information on the chemical reactivity of molecule and also to describe the intermolecular interactions. All these studies help us a lot in determining the reactivity of the mentioned compounds. Finally, docking calculations were carried out to determine the pharmaceutical activities of the chloroquine derivatives against coronavirus diseases. The choice of these ligands was based on their antiviral activities.

© 2020 The Author(s). Published by Elsevier B.V. on behalf of King Saud University. This is an open access article under the CC BY-NC-ND license (http://creativecommons.org/licenses/by-nc-nd/4.0/).

1. Introduction

In late December 2019, the coronavirus (Covid and R Team, 2019) was first reported in humans in Wuhan, China, and appeared as a rapidly spreading pandemic (Wang et al., 2020; Dong et al., 2020). About 46 million people worldwide have been infected as of 1, November 2020, and over 1 197 000 have died. It is worthy to mention that this pandemic has the same symptoms as a flue. Fatigue, fever, headache, runny nose and dry cough are the principal clinical symptoms of COVID-19. Thus far, there is no effective antiviral medication or vaccine against COVID-19 virus has been developed. Where the World Health Organization announced it as one of the most dangerous health catastrophes in human history (Bheenaveni, 2020) since this virus is accelerating very quickly more than predicted by experts (Al Shamsi et al., 2019). Therefore, searching for effective antiviral agents to battle against this virus is urgently needed. In this context, our investigations are destined for the development of therapeutic agents for COVID-19 diseases. Many scientists are working on the designing of efficacious antiviral agents with few aspect effects. Where recent research informed an inhibitor effect of the chloroquine and its derivatives on the growth of coronavirus (Gautret et al., 2020; Romano et al., 2020; Lecuit, 2020). Clinical trials have been done on Chinese patients COVID-19; have shown that the chloroquine has a great effect in terms of clinical results and viral clearance, in comparison to the control groups (Gautret et al., 2020). They have been proposed as a potential antiviral for the treatment of COVID-19 diseases based on their antiviral activities (Touret and X., 2020; Colson et al., 2020).

In this study, we evaluated the antiviral efficiency of two approved drugs which are chloroquine and chloroquine phosphate against the COVID-19 using molecular docking calculations. Docking is a technique of designing drug molecules via computer-aided by simulating the geometric of these molecules and their

* Corresponding authors.
  E-mail addresses: issaoui_noureddine@yahoo.fr (N. Issaoui), omar@ksu.edu.sa (O. Al-Dossary).

Peer review under responsibility of King Saud University.

Production and hosting by Elsevier

intermolecular forces (Noureddine et al., 2020a, 2020b). From this calculation, we can predict the different interactions between medications and targets which have an important role in the investigation of the mechanism of the effects of drugs. In this context, many nowadays papers is dedicated to searching in drug design using molecular docking studies (Jomaa et al., 2020; Sagaama et al., 2020a, 2020b; Issaoui et al., 2017). In the same frame, we can cite our previous paper (Romani et al., 2020) in which we used molecular docking analysis in the determination of the biological activity of the Niclosamide compound. As a result, the niclosamide is found to be a good inhibitor of the COVID-19 virus and can, therefore, be effective in controlling this disease.

The main contribution of this paper is to identify the potency of inhibition of chloroquine derivatives against COVID-19 virus by using a molecular docking study. To this end, we first determine the optimized structures of chloroquine and chloroquine phosphate molecules by using the density functional theory (DFT) at B3LYP/6-31G* level of theory. Utilizing optimized structures is more exact in docking calculations, which makes the program more trustworthy to be employed in structure-based drug design. Subsequently, their reactivities were foreseen at the same level of theory by using the frontier orbital studies (Brédas, 2014; Parr and Pearson, 1983). From this analysis, we can found the most reactive antiviral ligand. Moreover, molecular electrostatic potentials surfaces were carried out to investigate which are the most reactive nucleophilic and electrophilic regions of a molecule against reactive biological potentials. Docking calculations were performed using four structures of COVID-19 (PDB codes: 6 M03, 5R7Y, 5R81 and 6LU7) (http://www.rcsb.org/). Basing on the binding affinities and the different interactions that exist between amino acid residues and ligands, molecular docking results were discussed.

2. Computational details

2.1. DFT calculations

The GaussView program (GaussView, Guassian, Inc.) was utilized to model the initial structures of the chloroquine and the chloroquine phosphate molecules. Subsequently, their molecular geometries optimizations were carried out in the gas phase with the density functional theory (DFT) with the Gaussian 09 software package (Gaussian 09, Revision C.01, Frisch et al., 2009). All the quantum-chemical calculations have been performed via the hybrid B3LYP (Becke's three parameter hybrid functional with Lee-Yang-Parr correlation functional LYP (Lee et al., 1988; Becke, 1993) at 6-31G* basis set. Furthermore, several electronic properties for instance the frontier molecular orbitals, gap energies, reactivity descriptors were computed using TD-DFT approach (Liu et al., 2015; Becke, 1993). The density of states (DOS) plots was obtained by using Gauss-Sum software (O'Boyle et al., 2008).

2.2. Ligands and proteins preparation

The 3D structures of COVID-19 protein were retrieved from the RCSB PDB database (http://www.rcsb.org) (http://www.rcsb.org/). The Protein Data Bank (PDB) archive contains thousand protein structures obtained either by crystallography X-ray or by NMR. Concerning ligands, the 2D structures of chloroquine and chloroquine phosphate were extracted from the PubChem online database (https://pubchem.ncbi.nlm.nih.gov/). The ligands were saved in the MDL Mol file format. Then, they were converted to a PDB file format by using Accelrys Discovery Studio Visualizer (Visualizer, 2005). Thereafter, Rapid-Screening docking was carried out using iGEMDOCK program (Yang and Chen, 2004). It is a Drug Design System for docking calculations and screening by BioXGEM labs. All the trials were docked with a population size set to 800, with 80 generations and 10 solutions.

3. Results and discussion

3.1. Optimization of chloroquine and chloroquine phosphate

Optimized structures and numbering of atoms of chloroquine and chloroquine phosphate molecules are shown graphically in Figs. 1 and 2, obtained at B3LYP/6-31G* method. Table 1 illustrates their geometrical parameters such as the calculated total energies, the dipole moments, the RMS and the maximum Cartesian force. The global minimum energies are found to be -1326.0352 a.u (≈ -36083 eV) and -2614.3242 a.u (≈ -71139) for chloroquine and chloroquine phosphate, respectively. The RMS Cartesian force values are equal to $2.412\ 0.10^{-6}$, 0.04067 in chloroquine and chloroquine phosphate. Their maximum Cartesian forces are found to be $8.593\ 0.10^{-6}$ and 0.1449. The dipole moment of a molecule is given in the form of a three-dimensional vector and which reflects the molecular charge distribution. Hence, it can be employed as a descriptor to describe the charge movement throughout the molecule. As a result of DFT/B3LYP/6-31G* calculations, the highest dipole moment was observed for the chloroquine phosphate ($\sim$24.49 Debye) whereas the smallest one was observed for the chloroquine ($\sim$6.05 Debye). Of course, the adding of other atoms in the geometry of the chloroquine has an influence on their stability. We can notice that the chloroquine compound becomes more stable when adding the phosphate groups since the global minimum energy decreases. Also, the strong increase in the dipole moment value shows that the chloroquine is harder before adding the phosphate groups. Moreover, it promotes the formation of hydrogen bonds.

The optimized geometrical parameters of chloroquine derivatives have been determined by the above method and they are given in Tables 2 and 3 with the experimental bond angles and bond lengths. First, we observed that the theoretical bond lengths of chloroquine compound are almost similar with the experimental results (Busetta and Courseille, 1973), since the value of RMSD is very small (0.001 Å). The same applies to the bond angles which have an RMSD value equal to 0.298°. Same thing for the chloroquine phosphate, according to the result as collected in table 3 the bond distances and bond angles show good agreement with the experimental data (Albesa-Jové et al., 2008). We find that the RMSD value is equal to 0.065 Å for the bond distances and 3.382° for the bond angles. Results reveal that the carbon–carbon bond distances are found in the range 1.374–1.546 Å for C_{20}-C_{22} and C_5-C_7, respectively for the chloroquine. In the benzene ring (I), the carbon–carbon bond lengths C_{13}-C_{17}, C_{13}-C_{18}, C_{17}-C_{20}, C_{18}-C_{21}, C_{20}-C_{22} and C_{21}-C_{22} are 1.435, 1.418, 1.421, 1.378, 1.374 and 1.411 Å, respectively. The C–C bond alienation in the pyridine ring (II) is between 1.394 Å (for C_{12}-C_{16} bond) and 1.445 Å (for C_{12}-C_{13} bond). While, for chloroquine phosphate, the bond length between two carbon–carbon in the two rings is in the range 1.383–1.419 Å for benzene and 1.366 to 1.464 Å for pyridine ring. It is seen that the B3LYP calculated hydrogen bonding distances C–H vary from 1.009 Å (for N_3-H_{30}) to 1.099 Å (for C_5-H_{24}) for chloroquine and from 1.084 Å (for C_{10}-H_{27} bond) to 1.524 Å (for C_{21}-C_{22} bond) for chloroquine phosphate. Three nitrogen N atoms exist in the structure of chloroquine: the order of the N-C bond length is N_2-C_{10} > N_2-C_{11} > N_2-C_8 > N_3-C_7 > N_3-C_{12} > N_4-C_{17} > N_4-C_{19} having values 1.470 > 1.469 > 1.467 > 1.465 > 1.370 > 1.365 > 1.319 Å, respectively. The bond distance of N_3-H_{30} is equal to 1.009 Å. The bond angle of chloroquine between the C_7-N_3-H_{30} and C_{12}-N_3-H_{30} are $\sim$ 115.047° and $\sim$ 116.505°, respectively. Concerning the
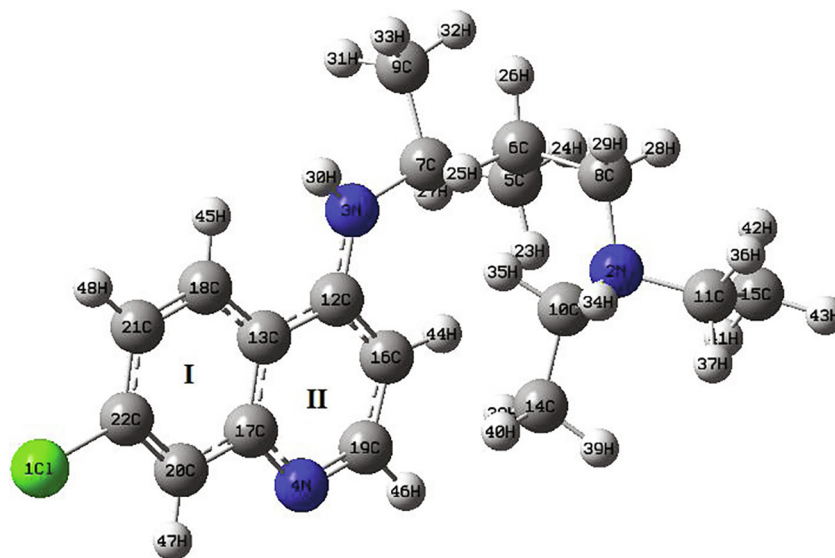
Fig. 1. Optimized structure of the chloroquine by using DFT/B3LYP/6-31G* method.
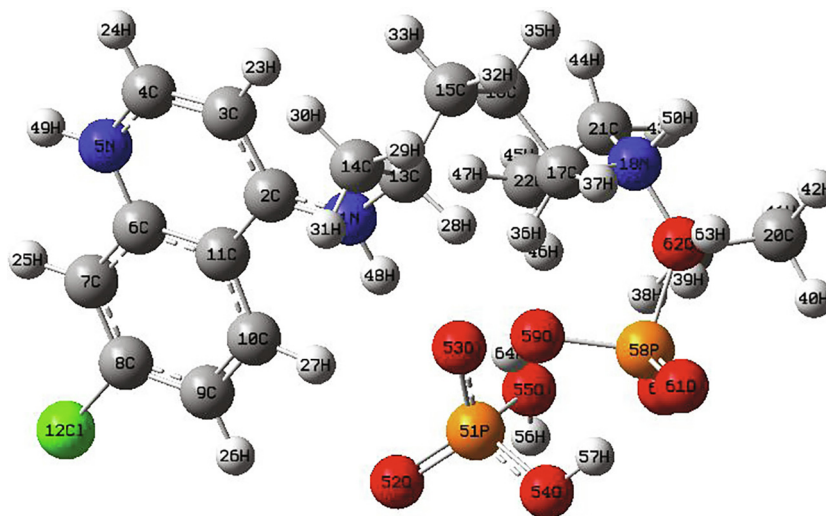

Fig. 2. Optimized structure of the chloroquine phosphate molecule.

Table 1
Calculated total energies (E), RMS Cartesian force, dipole moments (μ) and Maximum Cartesian force of chloroquine derivatives by using B3LYP/6-31G* level of theory.

B3LYP/6-31G* method				
Molecules	E (Hartree)	RMS Cartesian force	μ (D)	Maximum Cartesian force
Chloroquine	−1326.0352	2.412 0.10^{-6}	6.05	8.593 0.10^{-6}
Chloroquine phosphate	−2614.3242	0.04067	24.49	0.1449

chloroquine phosphate, we note that the single N_5-C_6 bond length of 1.387 Å for ring pyridine is higher than the N_5-C_4 double bond (1.353 Å). The P-O bond lengths are obtained to be in range 1.489–1.693 Å (for P_{58}-O_{61} and P_{58}-O_{62}). The O-P-O bond angles are reported in range 107.7–112.02°, whereas it is computed in range 102.543–124.278°. The C_8-Cl bond length is observed at 1.743 Å and calculated at 1.748 Å. The C_9-C_8-Cl and C_8-C_9-C_{10} bond angles are at 119.733° and 116.940°, respectively.

3.2. Frontier orbitals and quantum chemical calculations

Frontier molecular orbitals (FMOs) often play dominant roles in molecular systems. The fundamental idea of this theory can be abridged in the form of a simple rule telling the condition for a simple course of the reaction by the requirement of the maximal positive overlap between LUMO (empty state) and HOMO (filled state) orbitals. LUMO (lowest unoccupied molecular orbital) is directly related to electron affinity, while HOMO (highest occupied molecular orbital) is related to ionization potential (Xavier and Periandy, 2015; Abraham et al., 2017). These orbitals help to understand the chemical stability and the reactivity of the molecule (Asiri et al., 2011; Kosar, 2011). In order to predict the energetic behaviors and the reactivity of the chloroquine and the chloroquine phosphate against COVID-19 virus, the FMOs in the electronic transitions and their energies difference Eg are determined. A detailed analysis of the HOMOs and LUMOs orbitals is

Table 2

Calculated geometrical parameters for the chloroquine compound compared with the experimental ones by using B3LYP/6-31G* basis set.

Chloroquine					
Parameters	Experimental	Theoretical	Parameters	Experimental	Theoretical
Bond lengths (Å)					
$Cl-C_{22}$	1.755	1.760	$C_{12}-C_{16}$	1.393	1.394
N_2-C_8	1.469	1.467	$C_{13}-C_{17}$	1.432	1.432
N_2-C_{10}	1.460	1.470	$C_{13}-C_{18}$	1.418	1.418
N_2-C_{11}	1.498	1.469	$C_{14}-H_{38}$	1.095	1.095
N_3-C_7	1.500	1.465	$C_{14}-H_{39}$	1.096	1.096
N_3-C_{12}	1.371	1.370	$C_{14}-H_{40}$	1.070	1.096
N_3-H_{30}	1.009	1.009	$C_{15}-H_{41}$	1.095	1.095
N_4-C_{17}	1.344	1.365	$C_{15}-H_{42}$	1.096	1.096
N_4-C_{19}	1.368	1.320	$C_{15}-H_{43}$	1.096	1.096
C_5-C_6	1.534	1.534	$C_{16}-C_{19}$	1.407	1.407
C_5-C_7	1.546	1.546	$C_{16}-H_{44}$	1.065	1.083
C_5-H_{23}	1.095	1.095	$C_{17}-C_{20}$	1.500	1.421
C_5-H_{24}	1.100	1.100	$C_{18}-C_{21}$	1.374	1.378
C_6-C_8	1.554	1.538	$C_{18}-H_{45}$	1.087	1.087
C_6-H_{25}	1.098	1.098	$C_{19}-H_{46}$	1.090	1.090
C_6-H_{26}	1.099	1.098	$C_{20}-C_{22}$	1.374	1.374
C_7-C_9	1.546	1.533	$C_{20}-H_{47}$	1.034	1.084
C_7-H_{27}	1.097	1.097	$C_{21}-C_{22}$	1.411	1.411
C_8-H_{28}	1.096	1.096	$C_{21}-H_{48}$	1.084	1.084
C_8-H_{29}	1.149	1.108	$C_{10}-H_{35}$	1.078	1.095
C_9-H_{31}	1.095	1.095	$C_{11}-C_{15}$	1.319	1.530
C_9-H_{32}	1.095	1.095	$C_{11}-H_{36}$	1.208	1.108
C_9-H_{33}	1.097	1.097	$C_{11}-H_{37}$	1.056	1.095
$C_{10}-C_{14}$	1.525	1.530	$C_{12}-C_{13}$	1.442	1.445
$C_{10}-H_{34}$	1.108	1.108			
RMSD	0.001 Å				
Bond angles (°)					
$C_8-N_2-C_{10}$	112.84	112.103	$C_{15}-C_{11}-H_{37}$	108.29	108.196
$C_8-N_2-C_{11}$	112.23	112.200	$H_{36}-C_{11}-H_{37}$	105.89	106.039
$C_{10}-N_2-C_{11}$	111.78	111.972	$N_3-C_{12}-C_{13}$	120.83	120.095
$C_7-N_3-C_{12}$	124.77	125.707	$N_3-C_{12}-C_{16}$	124.34	123.092
$C_7-N_3-H_{30}$	115.049	115.048	$C_{13}-C_{12}-C_{16}$	116.790	116.790
$C_{12}-N_3-H_{30}$	116.50	116.505	$C_{12}-C_{13}-C_{17}$	117.68	117.797
$C_{17}-N_4-C_{19}$	116.07	116.079	$C_{12}-C_{13}-C_{18}$	124.08	123.818
$C_6-C_5-C_7$	115.89	115.643	$C_{17}-C_{13}-C_{18}$	118.16	118.383
$C_6-C_5-H_{23}$	107.62	107.782	$C_{10}-C_{14}-H_{38}$	110.36	110.369
$C_6-C_5-H_{24}$	109.60	109.535	$C_{10}-C_{14}-H_{39}$	113.36	112.214
$C_7-C_5-H_{23}$	109.22	109.218	$C_{10}-C_{14}-H_{40}$	110.08	110.289
$C_7-C_5-H_{24}$	107.15	107.798	$H_{38}-C_{14}-H_{39}$	107.9(1)	107.900
$H_{23}-C_5-H_{24}$	106.4(4)	106.496	$H_{38}-C_{14}-H_{40}$	108.5(3)	108.529
$C_5-C_6-C_8$	112.5(4)	112.597	$H_{39}-14-H_{40}$	107.410	107.410
$C_5-C_6-H_{25}$	109.59	109.519	$C_{11}-C_{15}-H_{41}$	110.79	110.273
$C_5-C_6-H_{26}$	110.24	110.944	$C_{11}-C_{15}-H_{42}$	112.3(4)	112.316
$C_8-C_6-H_{25}$	109.78	109.513	$C_{11}-C_{15}-H_{43}$	110.2(4)	110.276
$C_8-C_6-H_{26}$	107.46	107.750	$H_{41}-C_{15}-H_{42}$	107.8(3)	107.894
$H_{25}-C_6-H_{26}$	105.39	106.310	$H_{41}-C_{15}-H_{43}$	108.5(4)	108.564
$N_3-C_7-C_5$	113.57	113.473	$H_{42}-C_{15}-H_{43}$	107.3(4)	107.389
$N_3-C_7-C_9$	108.38	108.232	$C_{12}-C_{16}-C_{19}$	119.7354	119.736
$N_3-C_7-H_{27}$	106.58	106.584	$C_{12}-C_{16}-H_{44}$	121.70	121.300
$C_5-C_7-C_9$	113.83	113.289	$C_{19}-C_{16}-H_{44}$	118.952	118.959
$C_5-C_7-H_{27}$	107.54	107.546	$N_4-C_{17}-C_{13}$	123.19	123.911
$C_9-C_7-H_{27}$	107.33	107.331	$N_4-C_{17}-C_{20}$	116.9(4)	116.950
$N_2-C_8-C_6$	113.41	113.409	$C_{13}-C_{17}-C_{20}$	119.17	119.139
$N_2-C_8-H_{28}$	108.0(3)	108.072	$C_{13}-C_{18}-C_{21}$	121.72	121.739
$N_2-C_8-H_{29}$	111.43	111.344	$C_{13}-C_{18}-H_{45}$	120.37	120.684
$C_6-C_8-H_{28}$	108.78	108.140	$C_{21}-C_{18}-H_{45}$	117.562	117.561
$C_6-C_8-H_{29}$	109.59	109.436	$N_4-C_{19}-C_{16}$	125.27	125.662
$C_{28}-C_8-H_{29}$	106.122	106.122	$N_4-C_{19}-H_{46}$	114.49	115.975
$C_7-C_9-H_{31}$	110.742	110.742	$C_{16}-C_{19}-H_{46}$	118.3591	118.359
$C_7-C_9-H_{32}$	110.415	110.415	$C_{17}-C_{20}-C_{22}$	120.35	120.214
$C_7-C_9-H_{33}$	111.15	111.585	$C_{17}-C_{20}-H_{47}$	117.19	117.802
$H_{31}-C_9-H_{32}$	108.71	108.463	$C_{22}-C_{20}-H_{47}$	121.70	121.984
$H_{31}-C_9-H_{33}$	108.060	108.060	$C_{18}-C_{21}-C_{22}$	119.01	119.067
$H_{32}-C_9-H_{33}$	107.450	107.450	$C_{18}-C_{21}-H_{48}$	119.39	120.983
$N_2-C_{10}-C_{14}$	112.12	113.052	$C_{22}-C_{21}-H_{48}$	119.29	119.949
$N_2-C_{10}-H_{34}$	111.99	111.009	$Cl-C_{22}-C_{20}$	119.41	119.987
$N_2-C_{10}-H_{35}$	107.22	107.936	$Cl-C_{22}-C_{21}$	118.84	118.570
$C_{14}-C_{10}-H_{34}$	110.2(2)	110.284	$C_{20}-C_{22}-C_{21}$	121.72	121.442
$C_{14}-C_{10}-H_{35}$	109.41	108.216	$N_2-C_{11}-H_{36}$	111.71	111.218
$H_{34}-C_{10}-H_{35}$	105.45	106.030	$N_2-C_{11}-H_{37}$	107.46	107.769
$N_2-C_{11}-C_{15}$	113.3(2)	113.224	$C_{15}-C_{11}-H_{36}$	110.066	110.065
RMSD	0.298°				

Table 3
Calculated and observed geometrical parameters for the chloroquine phosphate.

Chloroquine phosphate					
Parameters	Experimental	Theoretical	Parameters	Experimental	Theoretical
Bond lengths (Å)					
N_1-C_2	1.409(2)	1.324	C_{17}-N_{18}	1.5069(6)	1.523
N_1-C_{13}	1.4967(9)	1.486	C_{17}-H_{36}	0.9994	1.095
N_1-H_{48}	1.0018	1.048	C_{17}-H_{37}	1.0005	1.094
C_2-C_3	1.415(3)	1.433	N_{18}-C_{19}	1.4980(6)	1.532
C_2-C_{11}	1.402(2)	1.464	N_{18}-C_{21}	1.5083(6)	1.516
C_3-C_4	1.400(3)	1.366	N_{18}-H_{50}	0.9995	1.025
C_3-H_{23}	1.000	1.079	C_{19}-C_{20}	1.5171(5)	1.521
C_4-N_5	1.366(1)	1.353	C_{19}-H_{38}	1.0010	1.091
C_4-H_{24}	0.999	1.084	C_{19}-H_{39}	1.0000	1.095
N_5-C_6	1.382(3)	1.387	C_{20}-H_{40}	1.0001	1.094
N_5-H_{49}	0.998	1.011	C_{20}-H_{41}	1.0001	1.096
C_6-C_7	1.403(1)	1.403	C_{20}-H_{42}	1.0000	1.098
C_6-C_{11}	1.417(3)	1.419	C_{21}-C_{22}	1.5296(5)	1.524
C_7-C_8	1.411(3)	1.386	C_{21}-H_{43}	1.0000	1.093
C_7-H_{25}	0.997	1.086	C_{21}-H_{44}	0.9998	1.094
C_8-C_9	1.396(3)	1.403	C_{22}-H_{45}	0.9998	1.095
C_8-Cl	1.743(3)	1.749	C_{22}-H_{46}	1.0009	1.092
C_9-C_{10}	1.373(1)	1.383	C_{22}-H_{47}	1.0002	1.093
C_9-H_{26}	0.999	1.085	H_{48}-O_{53}	1.517(8)	1.675
C_{10}-C_{11}	1.431(3)	1.412	P_{51}-O_{52}	1.513(5)	1.497
C_{10}-H_{27}	1.001	1.084	P_{51}-O_{53}	1.574(5)	1.548
C_{13}-C_{14}	1.5142(6)	1.536	P_{51}-O_{54}	1.560(5)	1.594
C_{13}-C_{15}	1.5417(7)	1.545	P_{51}-O_{55}	1.000	1.682
C_{13}-H_{28}	0.9998	1.093	O_{53}-H_{64}	1.554	1.782
C_{14}-H_{29}	0.9993	1.095	O_{54}-H_{57}	0.997	1.017
C_{14}-H_{30}	1.0000	1.095	O_{55}-H_{56}	0.9969	0.972
C_{14}-H_{31}	1.0002	1.094	H_{57}-O_{60}	1.5851	1.626
C_{15}-C_{16}	1.5092(6)	1.544	P_{58}-H_{59}	1.566(6)	1.645
C_{15}-H_{32}	1.0002	1.097	P_{58}-O_{60}	1.519(5)	1.528
C_{15}-H_{33}	1.0000	1.098	P_{58}-O_{61}	1.505(5)	1.489
C_{16}-C_{17}	1.5100(5)	1.531	P_{58}-O_{62}	1.578(6)	1.693
C_{16}-H_{34}	0.9995	1.096	H_{59}-H_{64}	1.005	0.991
C_{16}-H_{35}	0.9997	1.100	O_{62}-H_{63}	1.005	0.971
RMSD	0.065 Å				
Bond angles (°)					
C_2-N_1-C_{13}	121.5(1)	129.536	C_{16}-C_{17}-H_{36}	108.84	112.687
C_2-N_1-H_{48}	119.3	119.047	C_{16}-C_{17}-H_{37}	108.88	111.062
C_{13}-N_1-H_{48}	119.25	111.387	N_{18}-C_{17}-H_{36}	108.88	106.346
N_1-C_2-C_3	126.8(2)	123.005	N_{18}-C_{17}-H_{37}	108.83	104.285
N_1-C_2-C_{11}	115.6(2)	120.246	H_{36}-C_{17}-H_{37}	109.53	107.543
C_3-C_2-C_{11}	117.6(2)	116.748	C_{17}-N_{18}-C_{19}	105.42(4)	110.081
C_2-C_3-C_4	119.5(2)	120.770	C_{17}-N_{18}-C_{21}	117.16(4)	115.141
C_2-C_3-H_{23}	120.3	120.656	C_{17}-N_{18}-H_{50}	106.64	106.062
C_4-C_3-H_{23}	120.2	118.558	C_{19}-N_{18}-C_{21}	113.63(4)	113.264
C_3-C_4-N_5	122.7(2)	121.996	C_{19}-N_{18}-H_{50}	106.67	105.629
C_3-C_4-H_{24}	118.7	122.029	C_{21}-N_{18}-H_{50}	106.69	105.850
N_5-C_4-H_{24}	118.6	115.974	N_{18}-C_{19}-C_{20}	111.90(3)	111.886
C_4-N_5-C_6	119.1(2)	121.776	N_{18}-C_{19}-H_{38}	108.87	106.612
C_4-N_5-H_{49}	120.4	119.692	N_{18}-C_{19}-H_{39}	108.91	107.399
C_6-N_5-H_{49}	120.5	118.523	C_{20}-C_{19}-H_{38}	108.84	113.272
N_5-C_6-C_7	119.7(2)	119.461	C_{20}-C_{19}-H_{39}	108.80	111.196
N_5-C_6-C_{11}	119.9(2)	119.233	H_{38}-C_{19}-H_{39}	109.49	106.091
C_7-C_6-C_{11}	120.3(2)	121.305	C_{19}-C_{20}-H_{40}	109.48	107.585
C_6-C_7-C_8	118.6(2)	118.870	C_{19}-C_{20}-H_{41}	109.46	114.072
C_6-C_7-H_{25}	120.7	120.497	C_{19}-C_{20}-H_{42}	109.45	111.744
C_8-C_7-H_{25}	120.7	120.633	H_{40}-C_{20}-H_{41}	109.46	107.490
C_7-C_8-C_9	122.7(2)	121.420	H_{40}-C_{20}-H_{42}	109.46	106.889
C_7-C_8-Cl	120.4(2)	118.847	H_{41}-C_{20}-H_{42}	109.52	108.727
C_9-C_8-Cl	117.0(2)	119.733	N_{18}-C_{21}-C_{22}	115.92(3)	114.633
C_8-C_9-C_{10}	117.8(2)	119.188	N_{18}-C_{21}-H_{43}	107.84	105.833
C_8-C_9-H_{26}	121.1	122.471	N_{18}-C_{21}-H_{44}	107.83	106.449
C_{10}-C_9-H_{26}	121.1	118.339	C_{22}-C_{21}-H_{43}	107.80	110.976
C_9-C_{10}-C_{11}	122.5(2)	121.716	C_{22}-C_{21}-H_{44}	107.84	111.021
C_9-C_{10}-H_{27}	118.8	116.140	H_{43}-C_{21}-H_{44}	109.51	107.523
C_{11}-C_{10}-H_{27}	118.7	122.143	C_{21}-C_{22}-H_{45}	109.47	107.878
C_2-C_{11}-C_6	121.3(2)	119.448	C_{21}-C_{22}-H_{46}	109.43	113.139
C_2-C_{11}-C_{10}	120.7(2)	123.065	C_{21}-C_{22}-H_{47}	109.47	111.979
C_6-C_{11}-C_{10}	118.1(2)	117.483	H_{45}-C_{22}-H_{47}	109.52	108.829
N_1-C_{13}-C_{14}	112.18(5)	113.090	H_{45}-C_{22}-H_{47}	109.47	107.896
N_1-C_{13}-C_{15}	114.14(5)	114.908	H_{46}-C_{22}-H_{47}	109.47	106.971
N_1-C_{13}-H_{23}	105.70	102.804	N_1-H_{48}-O_{53}	109.7(4)	160.205

Table 3 (*continued*)

Chloroquine phosphate					
Parameters	Experimental	Theoretical	Parameters	Experimental	Theoretical
C_{14}-C_{13}-C_{15}	112.50(4)	112.432	O_{52}-P_{51}-O_{53}	109.6(4)	118.326
C_{14}-C_{13}-H_{23}	105.71	105.282	O_{52}-P_{51}-O_{54}	110.7(4)	112.552
C_{15}-C_{13}-H_{23}	105.77	107.166	O_{52}-P_{51}-O_{55}	107.7(3)	108.699
C_{13}-C_{14}-H_{30}	109.45	108.617	O_{53}-P_{51}-O_{54}	108.0(3)	109.174
C_{13}-C_{14}-H_{30}	109.49	114.029	O_{53}-P_{51}-O_{55}	111.0(3)	102.543
C_{13}-C_{14}-H_{31}	109.53	110.151	O_{54}-P_{51}-O_{55}	109.4	104.137
H_{29}-C_{14}-H_{30}	109.45	107.772	H_{48}-O_{53}-P_{51}	109.5	141.744
H_{29}-C_{14}-H_{31}	109.46	107.456	H_{48}-O_{53}-H_{64}	109.5(3)	96.870
H_{30}-C_{14}-H_{31}	109.44	108.592	P_{51}-O_{53}-H_{64}	118.544	113.169
C_{13}-C_{15}-C_{16}	116.02(4)	116.850	P_{51}-O_{54}-H_{57}	109.434	112.759
C_{13}-C_{15}-H_{32}	107.78	105.350	P_{51}-O_{55}-H_{56}	109.45	106.393
C_{13}-C_{15}-H_{33}	107.78	111.163	O_{54}-H_{57}-O_{60}	152.62	172.312
C_{16}-C_{15}-H_{32}	107.81	108.709	H_{59}-P_{58}-O_{60}	109.47	106.240
C_{16}-C_{15}-H_{33}	107.77	108.080	H_{59}-P_{58}- O_{61}	106.8(4)	111.947
H_{32}-C_{15}-H_{33}	109.57	106.135	H_{59}-P_{58}-O_{62}	108.7(4)	100.693
C_{15}-C_{16}-C_{17}	110.09(3)	112.212	O_{60}- P_{58}-O_{61}	111.1(4)	124.278
C_{15}-C_{16}-H_{34}	109.28	109.383	O_{60}- P_{58}-O_{62}	108.7(3)	104.611
C_{15}-C_{16}-H_{35}	109.31	106.991	O_{61}-P_{58}-O_{62}	112.02	106.329
C_{17}-C_{16}-H_{34}	109.35	110.830	P_{58}- H_{59}-H_{64}	109.5	109.330
C_{17}-C_{16}-H_{35}	109.31	110.727	H_{57}-O_{60}-P_{58}	112.0(4)	119.982
H_{34}-C_{16}-H_{35}	109.49	106.464	P_{58}-O_{60}-H_{63}	109.5	104.281
C_{16}-C_{17}-N_{18}	111.86(4)	114.339	O_{53}-H_{64}-H_{59}	161.56	162.347
RMSD	3.382°				

listed in Table 4, where orbital energies, energy band gap and reactivity descriptors (like electron affinity, chemical softness, ionization potential, chemical softness….) are reported. The gap between two energetic states describes the molecular chemical reactivity. The energies of the four important FMOs (HOMO, HOMO − 1, LUMO and LUMO + 1) were calculated via the TD-DFT approach with B3LYP/6-31G* level. Their 3D plots are illustrated in Figs. 3 and 4. It is clear from the figure of the chloroquine molecule that the HOMO and LUMO orbitals are localized essentially on the benzene and pyridine rings. The green color represents the negative phase; on the other hand the red color corresponds to the positive phase which is well clarified in the density of states (DOS) spectrum (Fig. 5). DOS spectrums characterize the energy levels per unit energy increment and its composing in energy. The displaying study per orbital shows that the green and the red lines in these curves correspond to the HOMO and LUMO energy levels, respectively. As a result, the energy level of the HOMO orbital is about −5.594 eV and the energy level of the LUMO orbital is about −1.115 eV. The HOMO-LUMO gap energy (Eg) of the chloroquine is equal to −4.479 eV. This low energy value pro-

motes the transfer of electrons in the chloroquine molecule. These values are compatible with those obtained by the DOS spectrum. The state HOMO-1 form another set of degenerate orbital −5.747 eV lower in energy than the HOMO set. As shown for the

Table 4
Calculated of some global reactivity descriptors of chloroquine derivatives.

Parameters	Chloroquine	Chloroquine phosphate
E_{LUMO}	−1.115	−2.599
E_{HOMO}	−5.594	−5.228
E_{HOMO}-E_{LUMO}	−4.479	−2.629
E_{LUMO+1}	−0.375	−1.579
E_{HOMO-1}	−5.747	−5.473
E_{HOMO-1}- E_{LUMO+1}	−5.372	−3.894
Reactivity descriptors		
Ionization potential (I)	5.594	5.228
Electron affinity (A)	1.115	2.599
Chemical hardness (η)	2.239	2.629
Chemical softness (ζ)	1.1195	1.3145
Electronegativity (χ)	3.3545	3.9135
Chemical potential	−3.3545	−3.9135
Electrophilicity index (ω)	2.512	2.912
Maximum charge transfer index	1.498	1.488

$I = -E_{HOMO}$, $A = -E_{LUMO}$, $\eta = (I–A)/2$, $\zeta = 1/2\eta$, $\chi = (I + A)/2$, $\mu = -(I + A)/2$, $\omega = \mu^2/2\eta$ and $\Delta N_{max.} = -\mu/\eta$.
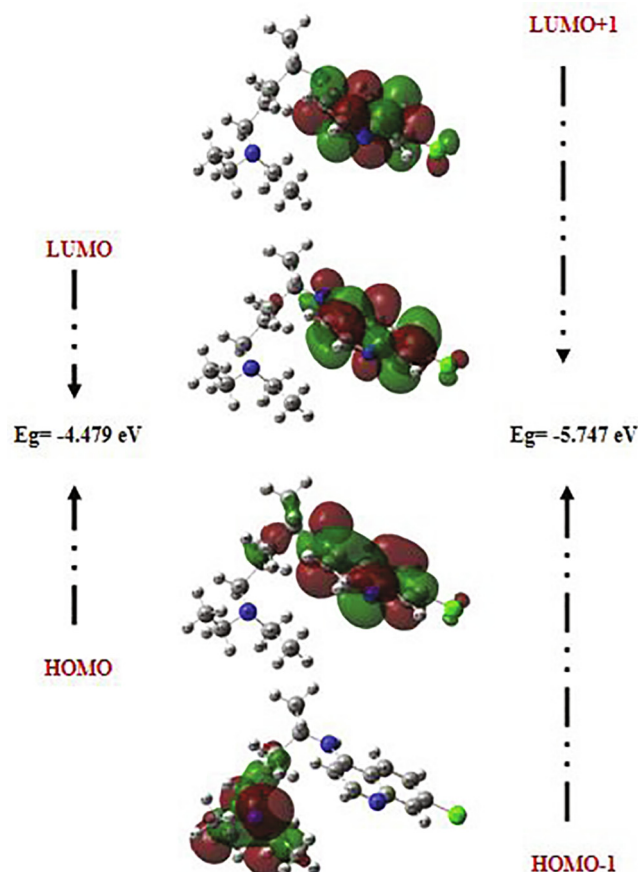

Fig. 3. The atomic orbital compositions of the HOMO, HOMO-1, LUMO and LUMO + 1 frontier molecular orbitals for chloroquine molecule.
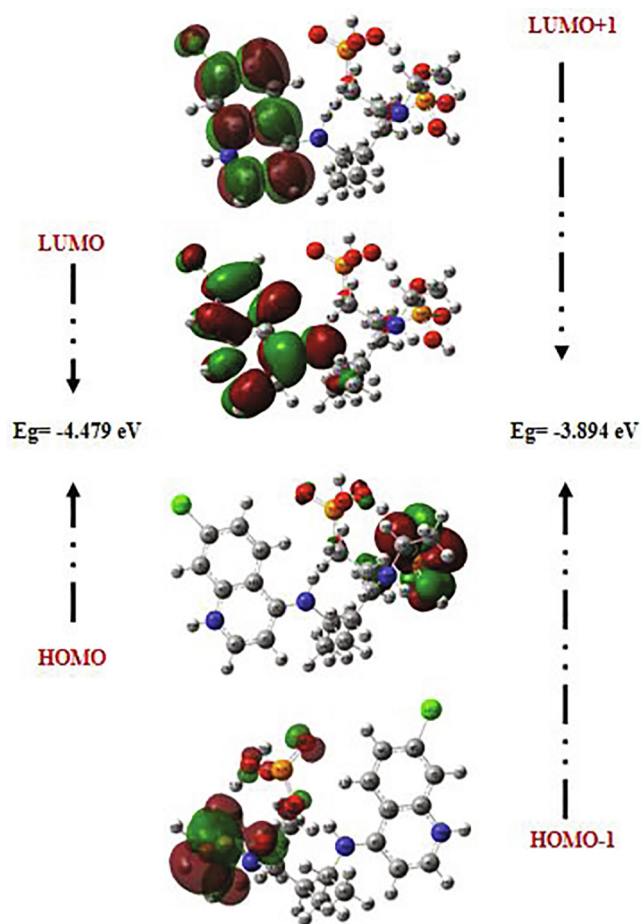
Fig. 4. The atomic orbital compositions of the HOMO, HOMO-1, LUMO and LUMO + 1 frontier molecular orbitals for chloroquine phosphate.

Fig. 5. DOS spectrum of chloroquine (a) and chloroquine phosphate (b) molecules.

chloroquine phosphate, LUMO orbital lying at −2.59 eV, located on all the atoms of the benzene and pyridine rings. The HOMO orbital is lying at −5.228 eV. Consequently, Eg is closed to −2.629 eV. The change observed here in the gap value from −4.479 eV to −2.629 eV in solution involves an expected high reactivity for the chloroquine phosphate. This decrease in gap energy makes the flow of electrons easier, so the molecule becomes soft and more reactive. We can also note that the chloroquine molecule is harder before adding the phosphate groups, given the energy value of gap. This result is in agreement with the strong increase in the dipole moment value of 6.05 Debye (of chloroquine) to 24.49 Debye (of chloroquine phosphate).

Using the energies of FMOs, we calculated the reactivity descriptors of chloroquine and chloroquine phosphate molecules. $A = -E_{LUMO}$: represent the electron affinity; $I = -E_{HOMO}$ represent the ionization potential and $\mu = 1/2(I + A)$ is the electronic chemical potential. The chemical hardness (η) is found to be 2.239 and 2.629 eV for chloroquine and chloroquine phosphate, respectively. The chemical softness (ζ) has been computed and found to be 1.1195 and 1.3145 eV^{-1}. Moreover, the electrophilicity index (ω) is about 2.512 eV for chlroquine and 2.912 eV for chloroquine phosphate. Based on the value found of the electrophilicity index, we can conclude that the chloroquine phosphate is a good electrophile better than chloroquine. Therefore, it is able to accept an electron doublet in order to form bonds with another reagent which is necessarily a nucleophile. Electronegativity is also determined ($\chi = (I + A)/2$) and it is found to be $\chi_{chloroquine}$ = 3.3545 eV and $\chi_{chloroquine\ phosphate}$ = 3.9135 eV.

3.3. Molecular electrostatic potential

The molecular electrostatic potential (MEP) is a well-established tool for the study of molecular reactive properties and to describe intermolecular interactions (Reed and Weinhold, 1985). It allows us to search the most reactive nucleophilic and electrophilic sites of a molecule against the reactive biological potentials (Gökce et al., 2013). These sites promote the formation of hydrogen bonds. The electrophilic site indicates a strong attraction, while the nucleophilic site indicates a strong repulsion. The electrostatic potential diagrams of chloroquine and chloroquine phosphate are illustrated in Fig. 6 at B3LYP/6-31G* method. MEP diagram gives negative, positive and neutral electrostatic potential regions in terms of color grading and is an indicator in the research of molecular structure properties. The red color represents the most electronegative electrostatic potential. That is, atoms in this region have a tendency to attract electrons (electrophilic). The blue color indicates the most electropositive potential (strong attraction) and the red color indicates the most electronegative potential (strong repulsion). Regions where the potentials are zero are denoted by green color. As a results, MEP surfaces varies between −5.504 0.10^{-2} a.u (deepest red) to 5.504 0.10^{-2} a.u (deepest blue) for chloroquine and between −0.116 a.u to 0.116 a.u for chloroquine phosphate. As can be seen, the MEP map of chloroquine molecule (Fig. 6a), a maximum positive region is localized on the

(a)

(b)
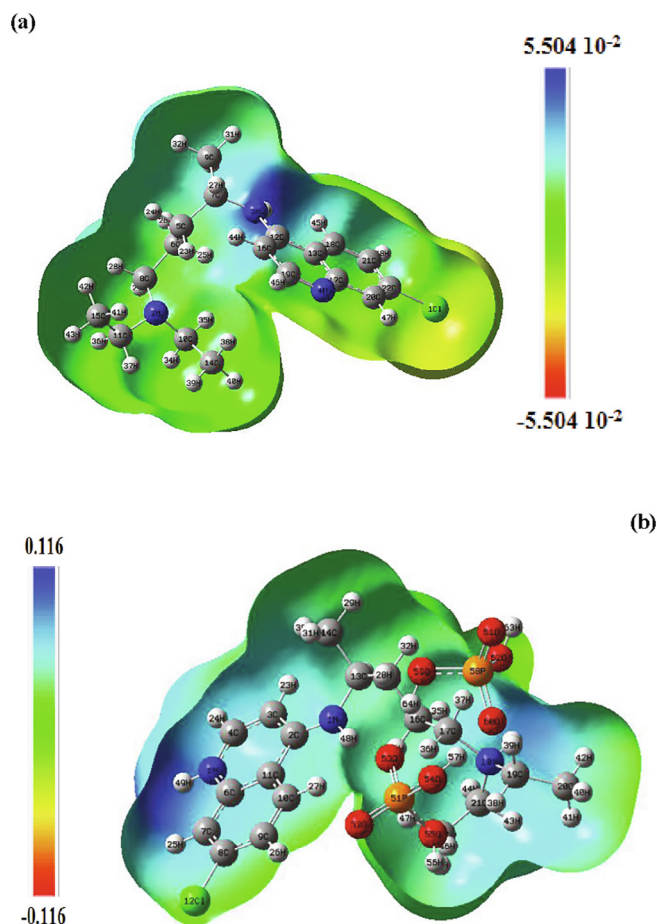
Fig. 6. Molecular electrostatic potential (MEP) maps of chloroquine and chloroquine phosphate molecules.

nitrogen N_3 and hydrogen H_{30} atoms indicating a possible site for electrophilic attack. The zero potential sites (green color) are found in the benzene ring. For the chloroquine phosphate (Fig. 6b), the positive potential (blue and light blue) sites are found in the benzene and pyridine rings (electrophilic reactivity). It can be inferred that the oxygen atoms O_{61} and O_{62} indicate the neutral potential of the molecule.

3.4. Molecular docking analysis

Molecular docking studies of chloroquine and chloroquine phosphate ligands were carried out with four structures of COVID-19 protein (PDB ID: 6 M03, 5R7Y, 5R81 and 6LU7). The two ligands were tested for drug-likeliness properties. Calculations were performed using the iGEMDOCK program through the generic evolutionary method (GA) and an empirical scoring function. Both ligands and target proteins structures were adapted with Discover Studio Visualizer software. All crystallographic water molecules were removed.

Our goal is to determine the modes of interaction of protein-ligand complexes while looking for favorable orientations for the binding of a ligand to a receptor (Duhovny et al., 2002; Seeliger and de Groot, 2010; Amin et al., 2010; Ahmed et al., 2013; Ghalla et al., 2018). In our case, the receptor represents the COVID-19 protein which has one or more specific active sites, more or less accessible. At each step, the interactions are affected and the best pose of the ligands is determined. 10 poses have been obtained; we have chosen the best pose with the lowest energy. These best poses, as

presented in Fig. 7, were selected for investigating the different types of interactions that introduce a biological signal.

3.4.1. Chloroquine

The examination of Table 5 revealed that the chloroquine ligand presented the highest total energy score with the target protein 6 M03 which is equal to −81.866 kcal/mol. Note that the total energy is the sum of the three energies interactions: VDW, hydrogen band and electronic. Van der Waals interaction is a potential energy of attraction between two molecules. It represents the sum of the energies of Keesom, London and Debye. The H-bond represents an interaction between two electronegative atoms. Generally, the energy of an H-bond is of the order of a few tens of KJ/Mol. It varies between 1 and 60 KJ/mol for neutral fragments, and sometimes it can reach higher values for some covalent bonds. The last interaction is electronic; they always take very low values compared to the other two interactions.

Chloroquine ligand posses the strongest van der Waals interaction E_{VDW} = -75.581 kcal/mol. The docking pose analysis showed that the chloroquine ligand is oriented with the VDW interactions surrounded by the chains of LEU-141, MET-165, PHE140, HIS163, GLN189, MET49, GLY143, THR25 and VAL42 binding residues in the 6 M03 protein. Also, it have the strongest H-bond interaction E_{H-bond} = -6.893 kcal/mol. The greater negative energy score suggests a more favorable binding mode. Table 6 presents the different interactions between the chloroquine ligand and proteins via the binding residues along with their bond length. Results obtained for protein targets show that the chloroquine ligand has bonded effectively with 6 M03 target sites with two remarkable carbon-hydrogen bond interactions. The mentioned compound is immensely bonded with active residues SER144 (Serine) and HIS164 (Histidine) by carbon-hydrogen bond interactions conduct to more antiviral activity. The first C—H bond interaction was identified between H_{46} atom and SER144 binding residues and the distance was found to be 2.61 Å. The second C—H bond interaction was identified between H_{27} and HIS164 with distance 2.27 Å. The hydrogen atom H_{30} linked to HIS41 amino residues via an alkyl interaction with bond length equal to 4.11 Å. Also, Pi-Sulfur, Pi-Alkyl and Pi-Anion interactions were observed surrounded by the amino acids CYS145, LEU27 and GLU166, having distances 3.99, 4.28 and 4.55 Å, respectively. These results have been well described in Figs. 8 and 9. Furthermore, chloroquine molecule showed total energy score of −77.498 kcal/mol against 5R7Y protein with VDW interaction (−70.605 kcal/mol) and hydrogen bond energy (−6.893 kcal/mol). Regarding the two other proteins (5R81 and 6LU7), the interaction energies are slightly weaker in comparison with the other ligands but as even remain important. The docking calculations led to the following results: the total energies scores are equal to −68.514 kcal/mol and −67.136 kcal/mol for 5R81 and 6LU7, respectively. The van der Waals interactions were found to be E_{VDW} (for 5R81) = −65.014 kcal/mol and E_{VDW} (for 6LU7) = −64.988 kcal/mol. Additionally, the hydrogen bond interactions exhibiting values of −3.500 and −2.147 kcal/mol for 5R81 and 6LU7 receptors. In the chloroquine-5R7Y complex, a Pi-Anion and Pi-Sulfur interactions wrapped by the amino acids GLU166 and CYS145 were formed with bond lengths 4.42 and 4.03 Å. C_{15} atom made two Alkyl interactions with A:CYS145 and A:LEU27 residues and having distances 3.99 and 4.07 Å. Also, C_{15} interact with A:HIS41 via a Pi-Alkyl interaction (bond length = 3.88 Å). A: SER144 and A:HIS164 amino residues form two carbon-hydrogen bond interactions with H_{46} and H_{27} atoms. Their bonding distances are found to be 2.53 Å and 1.98 Å, respectively. In 5R81virus, A: MET165 and A:MET49 amino residues are involved in the alkyl interaction with C_{10} and C_{15} atoms having bond length 4.43 and 3.96 Å. Pyridine group formed Pi-Alkyl, Pi-Sulfur and Pi-Donor hydrogen bond interactions with A:LEU27 (5.13 Å), A:CYS145
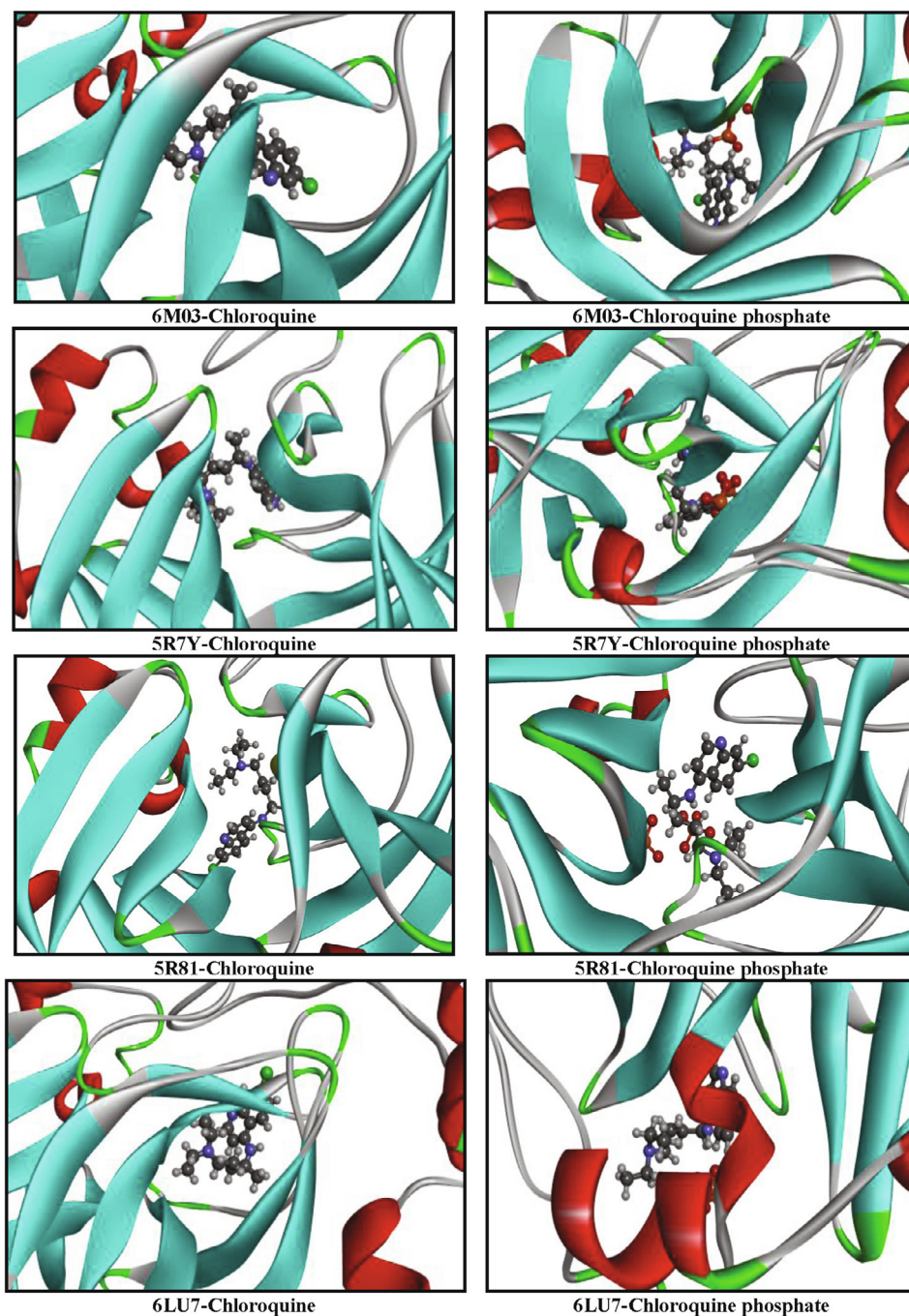
Fig. 7. Orientation of chloroquine and chloroquine phosphate in the active sites of COVID-19 proteins.

(4.08 Å) and A:CYS143 (3.80 Å) residues, respectively. Another Pi-Alkyl interaction is also seen which contributed by A:HIS41 with C_{15} atom, indicating distance 4.25 Å. For the last ligand 6LU7, the LEU141 (2.38 Å), the ASN142 (3.02 Å) and the HIS163 (2.47 Å) amino acids formed a C—H bond interactions with H_{29}, H_{27} and H_{28} atoms of chloroquine. In addition to these weak interactions there are two alkyl interactions; one between PRO168 residues and the Cl atom and the second one is in between CYS145 and the N_2 atom, indicating bond distance 3.63 and 4.35 Å, respectively. Subsequently, the H_{30} atom exhibit a conventional-H bond interaction with GLU166 residues and bonding distance is 2.22 Å.

In order to upgrade the recognition of the interactions existing between receptor and ligand, the affinities of these complexes were calculated by using AutoDockTools (ADT) (Morris et al.,

2008). These affinities describe the strength of a non-covalent interaction between the ligand and its target which binding to a site on its surface. It is premised on the numeral and the nature of the physicochemical interactions. As illustrated in Table 5; the affinities values (in ultimate value) of chloroquine are found to be in the order of 6.7 > 6.6 > 6.1 kcal/mol for (6 M03 and 5R81), 5R7Y and 6LU7, respectively.

3.4.2. Chloroquine phosphate

According to the energetic related results of the docking calculations and the corresponding docking positions, the chloroquine phosphate has better binding interaction with 5R7Y protein (as seen in Table 5 and Fig. 7). This protein strongly interacts with the mentioned ligand, resulting in high inhibition potency. It

Table 5
Docking results of chloroquine and chloroquine phosphate in COVID-19 protein.

Chloroquine				
Ligands	6 M03	5R7Y	5R81	6LU7
Total energy	−81.866	−77.498	−68.514	−67.136
VDW	−75.581	−70.605	−65.014	−64.988
H-bond	−6.285	−6.893	−3.500	−2.147
Electronic	0	0	0	0
Affinity	−6.7	−6.6	−6.7	−6.1
Chloroquine phosphate				
Ligands	5R7Y	6 M03	5R81	6LU7
Total energy	−99.119	−88.686	−84.817	−82.663
VDW	−66.409	−55.450	−79.862	−69.861
H-bond	−29.499	−30.505	−4.9547	−12.802
Electronic	−3.210	−2.731	0	0
Affinity	−4.5	−3.5	−3.5	−3.6

Table 6
Amino acid residues-chloroquine interactions.

Ligand	Target protein	Binding residue	Type	Atoms	Bond length (Å)	Interactions
Chloroquine	5R7Y	A:GLU166	GlutamicAcid	Benzene	4.42	Pi-Anion
		A:CYS145	Cysteine	Pyridine	4.03	Pi-Sulfur
		A:CYS145	Cysteine	C_{15}	3.99	Alkyl
		A:LEU27	Leucine	C_{15}	4.07	Alkyl
		A:HIS41	Histidine	C_{15}	3.88	Pi-Alkyl
		A:SER144	Serine	H_{46}	2.53	Carbon-H bond
		A:HIS164	Histidine	H_{27}	1.98	Carbon-H bond
	6 M03	A:CYS145	Cysteine	Pyridine	3.99	Pi-Sulfur
		A:GLU166	GlutamicAcid	Pyridine	4.55	Pi-Anion
		A:HIS41	Histidine	H_{30}	4.11	Alkyl
		A:LEU27	Histidine	H_{30}	4.28	Pi-Alkyl
		A:SER144	Serine	H_{46}	2.61	Carbon-hydrogen bond
		A:HIS164	Histidine	H_{27}	2.27	Carbon-hydrogen bond
	6LU7	A:LEU141	Leucine	H_{29}	2.38	C—H bond
		A:ASN142	Asparagine	H_{27}	3.02	C—H bond
		A:HIS163	Histidine	H_{28}	2.47	C—H bond
		A:PRO168	Proline	Cl	3.63	Alkyl
		A:CYS145	Cysteine	N_2	4.35	Alkyl
		A:GLU166	GlutamicAcid	H_{30}	2.22	Conventional H-bond
	5R81	A:MET165	Methionine	C_{10}	4.43	Alkyl
		A:MET49	Methionine	C_{15}	3.96	Alkyl
		A:HIS41	Histidine	C_{15}	4.25	Pi-Alkyl
		A:LEU27	Histidine	Pyridine	5.13	Pi-Alkyl
		A:CYS145	Cysteine	Pyridine	4.08	Pi-Sulfur
		A:CYS143	GlutamicAcid	Pyridine	3.80	Pi-Donor H-bond

presented the highest total energy value of −99.119 kcal/mol with a −66.409 kcal/mol van der Waals interaction, also along with important hydrogen and electronic energies equal to −29.499 and −3.210 kcal/mol, respectively. Thereafter, we show that the binding affinities of chloroquine phosphate-6 M03 complex exhibit total energy score equal to −88.686 kcal/mol with E_{VDW} = −55.450 kcal/mol, $E_{H\text{-}bond}$ = −30.505 kcal/mol and $E_{electronic}$ = −2.731 kcal/mol. The total energies scores of 5R81 and 6LU7 proteins are found to be −84.817 and −82.663 kcal/mol, respectively. As clearly seen, docking calculations led to the following results: the H-bond interaction equal to −4.954 and −12.802 kcal/mol and their VDW interaction were −79.862 and −69.861 kcal/mol, respectively. For PDB ID: 5R7Y, as shown in Table 7, the amino acid A:MET49 and A:MET165 residues were involved in alkyl interaction with C_{15} atom with 4.52 and 4.39 Å bond length, respectively. Likewise, C_{15} atom was linked to A:HIS41 (4.40 Å) throughout pi-alkyl interaction. Moreover, oxygen atom O_{55} showed a conventional hydrogen bond with amino acid A:GLU166 having distance 2.65 Å. The pyridine group present a Pi-Donor H-bond with A:ASN142, indicating 4.19 Å bond length. For the second 6 M03-chloroquine phosphate complex, A:MET49 interacted with C_{22} and C_{20} atoms via alkyl interaction with 3.17 and 4.05 Å bond length. A pi-alkyl inter-

action was also being formed between A:HIS41 residues and C_{20} (3.58 Å). In addition, H_{63} atom (2.45 Å) involve in carbon H-bond with A:HIS164 amino acid. The pyridine ring exhibited pi-donor H-bond interaction with A:ASN142 having 3.79 Å distance. Then, O_{54} atom has a conventional H-bond interaction with A:GLU166 residues with distance value 3.27 Å. Amino acids A:HIS41 and A:HIS145 forms Pi-Alkyl interactions with Cl atom (4.87 Å) and benzene ring (4.73 Å) for PDB ID: 6LU7. As well, the Cl atom interacts with A:HIS145 via an Alkyl interaction with 3.54 Å distance. The H_{63} and H_{24} atoms have a carbon H-bond interactions with A:GLN189 and A:HIS163 residues with distances values 2.74 Å and 2.95 Å, respectively. Finally, the other amino acids A:ASN142 and A:SER144 forms two conventional H-bond interactions with H_{48} (2.78 Å) and N_5 (2.93 Å) atoms. For the last 5R81-chloroquine phosphate complex, an Alkyl interaction was observed between A:PRO168 amino acid residues and Cl atom having 5.02 Å bond length. In addition, two Pi-Alkyl interactions are performed between A:MET165 and A:MET49 residues and pyridine ring. Their bond lengths are equal to 4.40 and 4.67 Å, respectively. A:HIS41, A:THR190 and A:HIS41 amino acid residues interacted with C_{15}, Cl and pyridine ring via Pi-Sigma, halogen and Pi-Pi T shaped interactions, showed distances ranging from 3.04 to 5.01 Å. Chloroquine
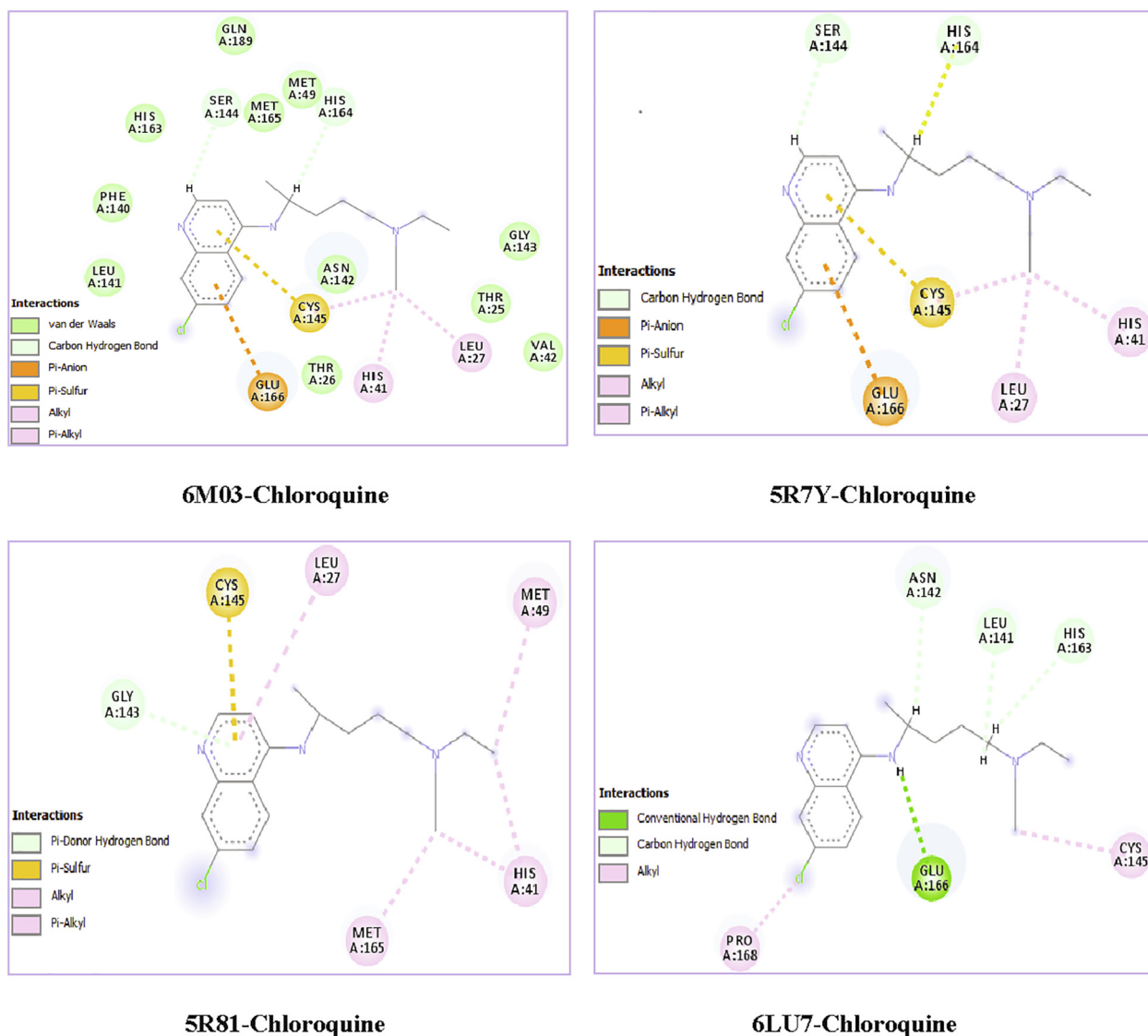
Fig. 8. 2D visual representations of chloroquine ligand-COVID-19 proteins.

phosphate present weaker affinities -4.5 kcal.mol^{-1} (for 5R7Y), -3.6 kcal.mol^{-1} (6LU7), -3.5 kcal.mol^{-1} (5R81), -3.5 kcal.mol^{-1} (6 M03).

- The results obtained show that the chloroquine penetrates well into the active areas of the protein. Therefore, it can be considered to be a potent inhibitor against COVID-19 diseases. But the chloroquine phosphate molecule showed a better activity rather than chloroquine since it interacts stronger with the receptor. This can be justified by the effect of the addition of the phosphate groups.

3.5. Hybridization effect

Of course, each compound has its own characteristics that distinguish it from the rest. The chloroquine phosphate is initially made up of chloroquine. Evidently, the adding of other atoms in the geometry of the chloroquine has an influence on their stability. The chloroquine compound becomes more stable when adding the phosphate groups since the global minimum energy decreases. Moreover, the smallest dipole moment was obtained for the chloroquine whereas the highest one was obtained for the chloro-

quine phosphate. This increase shows that the chloroquine is harder before adding the phosphate groups and also it promotes the formation of hydrogen bonds. We also find that by adding phosphate group the gap energy decreases, which involves a high reactivity for the chloroquine phosphate. This decrease in gap energy makes the flow of electrons easier, so the molecule becomes soft and more reactive.

4. Conclusion

Given their high efficiency in the treatment against COVID-19 pandemic, chloroquine derivatives have been studied combining DFT method and molecular docking calculations. The optimized molecular structures of chloroquine and chloroquine phosphate have been carried out using DFT/B3LYP/6-31G* method and their geometrical parameters were also determined. The comparison of the observed and calculated results showed a good agreement. Molecular properties such as frontiers orbitals, gap energies and reactivity descriptors have also been discussed. Results reveal that the addition of the sulfate group resulted in a decrease in the gap energy, which involves an expected high reactivity for the chloroquine phosphate. This decrease in gap energy makes the flow of

(A)

5R7Y-Chloroquine

6M03- Chloroquine

6LU7- Chloroquine

5R81-Chloroquine
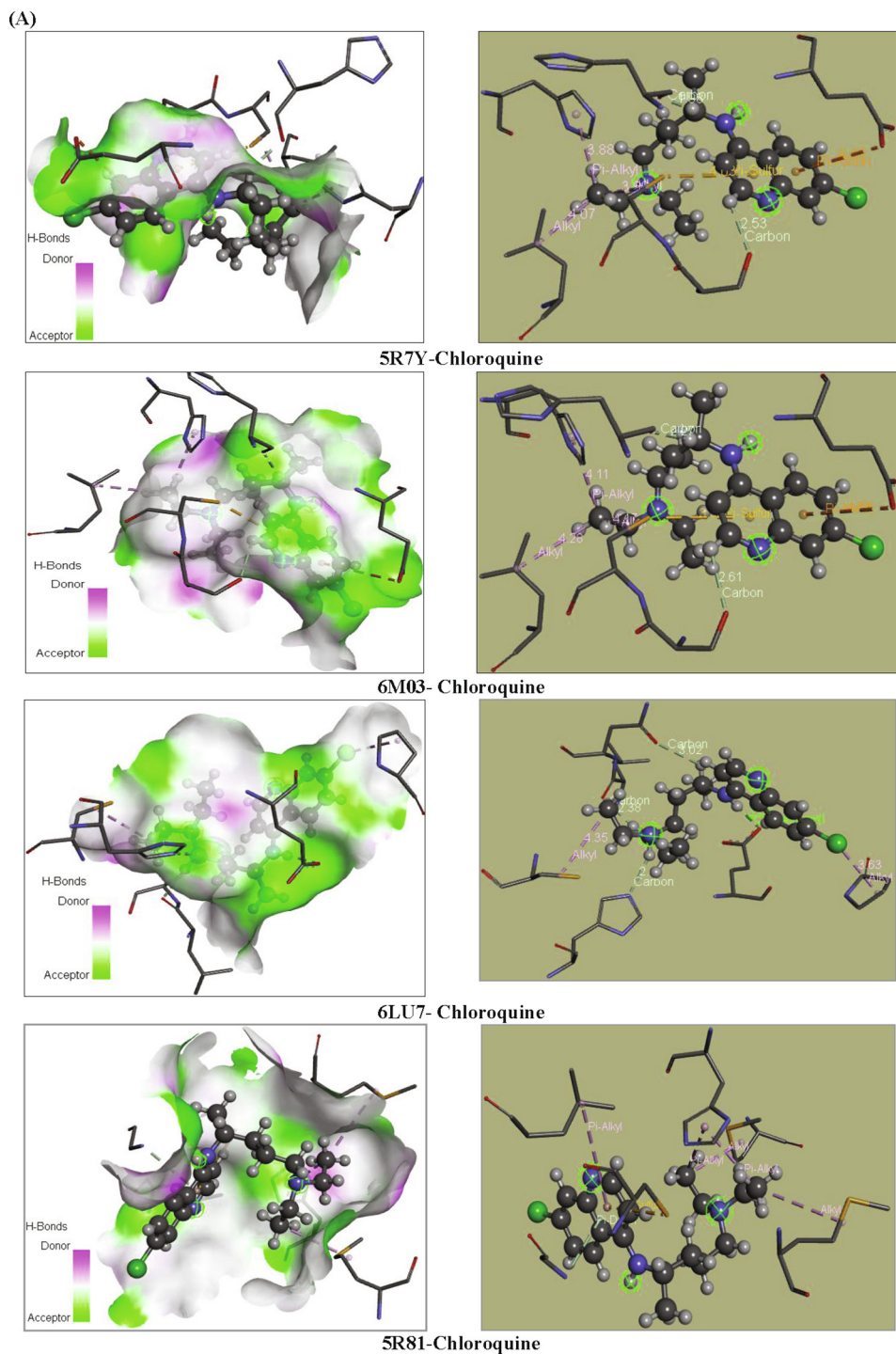
Fig. 9. Different interactions between ligand and their receptor.

electrons easier, so the molecule becomes soft and more reactive. The density of states (DOS) was determined and it allowed bettering describing the border orbitals. Thereafter, the calculated MEP maps show the positive potential sites are favorable for nucleophilic attack, whereas the negative potential sites are favorable for the electrophilic attack. Docking results were discussed based on the different interactions between the ligands and proteins. The chloroquine derivatives are found to be a good inhibitor of COVID-19 virus and can, therefore, be effective in controlling this disease. We found that chloroquine phosphate was considered to be the best inhibitor of coronavirus pandemic.

Funding

Declaration of Competing Interest

The authors declare that they have no known competing financial interests or personal relationships that could have appeared to influence the work reported in this paper.

(B)

5R7Y-Chloroquine phosphate

6M03-Chloroquine phosphate

6LU7-Chloroquine phosphate

5R81-Chloroquine phosphate
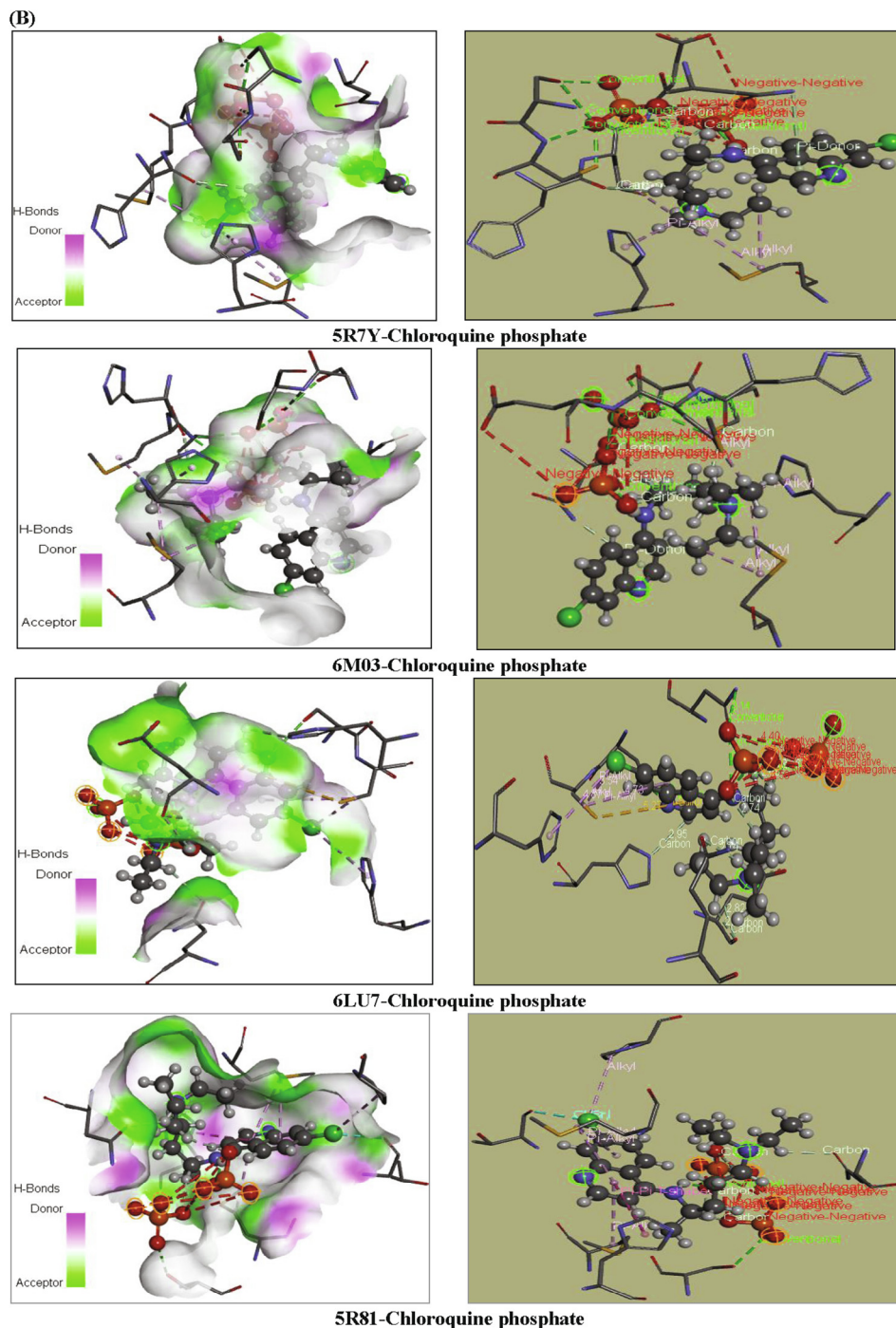
Fig. 9 (*continued*)

Table 7
Amino acid residues-chloroquine phosphate interactions.

Ligand	Target protein	Binding residue	Type	Atoms	Bond length (Å)	Interactions
Chloroquine phosphate	5R7Y	A:MET49	Methionine	C_{15}	4.52	Alkyl
		A:MET165	Methionine	C_{15}	4.39	Alkyl
		A:HIS41	Histidine	C_{15}	4.40	Pi-Alkyl
		A:GLU166	GlutamicAcid Asparagine	O_{55}	2.65	Conventional H-bond
		A:ASN142		Pyridine	4.19	Pi-Donor H-bond
	6 M03	A:MET49	Methionine	C_{22}	3.17	Alkyl
		A:MET49	Methionine	C_{20}	4.05	Alkyl
		A:HIS41	Histidine	C_{20}	3.58	Pi-Alkyl
		A:HIS164	Histidine	H_{63}	2.45	Carbon H-bond

13

Table 7 (*continued*)

Ligand	Target protein	Binding residue	Type	Atoms	Bond length (Å)	Interactions
		A:ASN142	Asparagine	Pyridine	3.79	Pi-Donor H-bond
		A:GLU166	GlutamicAcid	O_{54}	3.27	Conventional H-bond
	6LU7	A:HIS41	Histidine	Cl	4.87	Pi-Alkyl
		A:HIS145	Histidine	Benzene	4.73	Pi-Alkyl
		A:HIS145	Histidine	Cl	3.54	Alkyl
		A:GLN189	Glutamine	H_{63}	2.74	Carbon-hydrogen bond
		A:HIS163	Histidine	H_{24}	2.95	Carbon-hydrogen bond
		A:ASN142	Asparagine	H_{48}	2.78	Conventional H-bond Conventional H-bond
		A:SER144	Serine	N_5	2.93	
	5R81	A:PRO168	Proline	Cl	5.02	Alkyl
		A:MET165	Methionine	Pyridine	4.40	Pi-Alkyl
		A:MET49	Methionine	Pyridine	4.67	Pi-Alkyl
		A:HIS41	Histidine	C_{15}	3.81	Pi-Sigma
		A:THR190	Threonine	Cl	3.04	Halogen
		A:HIS41	Histidine	Pyridine	5.01	Pi-Pi T shaped

References

Abraham, Christina Susan, Prasana, Johanan Christian, Muthu, S., 2017. Quantum mechanical, spectroscopic and docking studies of 2-Amino-3-bromo-5-nitropyridine by Density Functional Method. Spectrochim. Acta Part A 181, 153–163.

Ahmed, L., Rasulev, B., Turabekova, M., Leszczynska, D., Leszczynski, J., 2013. Receptor-and ligand-based study of fullerene analogues: comprehensive computational approach including quantum-chemical, QSAR and molecular docking simulations. Org. Biomol. Chem. 11, 5798–5808.

Al Shamsi, H.O., Alhazzani, W., Alhuraiji, A., Coomes, E.A., Chemaly, R.F., Almuhanna, M., Meyers, B.M., 2019. A practical approach to the management of cancer patients during the novel coronavirus disease, (COVID-19) pandemic: an international collaborative group. Oncologist 25 (2020), 936.

Albesa-Jové, D., Pan, Z., Harris, K.D., Uekusa, H., 2008. A solid-state dehydration process associated with a significant change in the topology of dihydrogen phosphate chains, established from powder X-ray diffraction. Cryst Growth Des. 8, 3641–3645. https://doi.org/10.1021/cg800226e.

Amin, K., Kamel, M., Anwar, M., Khedr, M., Syam, Y., 2010. Synthesis, biological evaluation and molecular docking of novel series of spiro [(2H, 3H) quinazoline-2, 1′-cyclohexan]-4 (1H)-one derivatives as anti-inflammatory and analgesic agents. Eur. J. Med. Chem. 45, 2117–2131.

Asiri, A.M., Karabacak, M., Kurt, M., Alamry, K.A., 2011. Spectrochim. Acta A 82, 444–455.

Becke, A.D., 1993. Becke's three parameter hybrid method using the LYP correlation functional. J. Chem. Phys. 98, 5648–5652.

Becke, A.D., 1993. J. Chem. Phys. 98, 5648–5652.

Bheenaveni, R.S., 2020. India's indigenous idea of herd immunity: the solution for COVID-19. Tradit. Med. Res. 5, 182–187.

Brédas, J.-L., 2014. Mind the gap. Mater. Horizons 1, 17–19.

Busetta, B., Courseille, C., 1973. Structure cristallines et moléculaires de trois formes polymorphes de l'oestrone. Acta Crystallogr. B Struct. Cryst. Cryst. Chem. 29, 298–313. https://doi.org/10.1107/S0567740873002384.

Colson, P., Rolain, J.M., Lagier, J.C., Brouqui, P., Raoult, D., 2020. Chloroquine and hydroxychloroquine as available weapons to fight COVID-19. Int. J. Antimicrob. Agents 105932.

Covid, C.D.C., R. Team, 2019. Severe outcomes among patients with coronavirus disease (COVID-19)—United States. MMWR Morb. Mortal Wkly. 69 (2020), 343–346.

Dong, Y., Mo, X., Hu, Y., Qi, X., Jiang, F., Jiang, Z., Tong, S., 2020. Epidemiological characteristics of 2143 pediatric patients with 2019 coronavirus disease in China. Pediatrics.

D. Duhovny, R. Nussinov, H.J. Wolfson, Efficient unbound docking of rigid molecules, (2002).

Gaussian 09, Revision C.01, Frisch, M.J.; Trucks, G.W.; Schlegel, H.B.; Scuseria, G.E.; Robb, M.A.; Cheeseman, J.R.; Scalmani, G.; Barone, V.; Mennucci, B.; Petersson, G.A.; Nakatsuji, H.; Caricato, M.; Li, X.; Hratchian, H.P.; Izmaylov, A.F.; Bloino, J.; Zheng, G.; Sonnenberg, J.L.; Hada, M.; Ehara, M.; Toyota, K.; Fukuda, R.; Hasegawa, J.; Ishida, M.; Nakajima, T.; Honda, Y.; Kitao, O.; Nakai, H.; Vreven, T.; Montgomery, J.A., Jr.; Peralta, J.E.; Ogliaro, F.; Bearpark, M.; Heyd, J.J.; Brothers, E.; Kudin, K.N.; Staroverov, V.N.; Kobayashi, R.; Normand, J.; Raghavachari, K.; Rendell, A.; Burant, J.C.; Iyengar, S.S.; Tomasi, J.; Cossi, M.; Rega, N.; Millam, N.J.; Klene, M.; Knox, J.E.; Cross, J.B.; Bakken, V.;Adamo, C.; Jaramillo, J.; Gomperts, R.; Stratmann, R.E.; Yazyev, O.; Austin, A. J.; Cammi, R.; Pomelli, C.; Ochterski, J. W.; Martin, R.L.; Morokuma, K.; Zakrzewski, V.G.; Voth, G.A. Salvador, P.; Dannenberg, J.J.; Dapprich, S.; Daniels, A.D.; Farkas, Ö.; Foresman, J.B.; Ortiz, J.V. Cioslowski, J.; Fox, D.J. Gaussian, Inc., Wallingford CT (2009).

GaussView, Guassian, Inc. (Carnergie Office Parck-Building6 Pittsburgh PA 151064 USA), Copyright © 2000-2003 Semichem. Inc.

Gautret, P., Lagier, J.C., Parola, P., Meddeb, L., Mailhe, M., Doudier, B., Honore, S., 2020. Hydroxychloroquine and azithromycin as a treatment of COVID-19: results of an open-label non-randomized clinical trial. Int. J. Antimicrob. Agents 105949.

Gautret, P., Lagier, J.C., Parola, P., Meddeb, L., Mailhe, M., Doudier, B., Honoré, S., 2020. Hydroxychloroquine and azithromycin as a treatment of COVID-19: results of an open-label non-randomized clinical trial. Int. J. Antimicrob. Agents 105949.

Ghalla, H., Issaoui, N., Bardak, F., Atac, A., 2018. Intermolecular interactions and molecular docking investigations on 4-methoxybenzaldehyde. Comput. Mater. Sci 149, 291–300.

Gökce, H., Bahceli, S., Akyıldırım, O., Yüksel, H., Kol, O.G., 2013. Lett. Org. Chem. 10, 395–441.

http://www.rcsb.org/.

https://pubchem.ncbi.nlm.nih.gov/.

Issaoui, N., Ghalla, H., Bardak, F., Karabacak, M., Dlala, N.A., Flakus, H.T., Oujia, B., 2017. Combined experimental and theoretical studies on the molecular structures, spectroscopy, and inhibitor activity of 3-(2-thienyl) acrylic acid through AIM, NBO, FT-IR, FT-Raman, UV and HOMO-LUMO analyses, and molecular docking. J. Mol. Struct. 1130, 659–668.

Jomaa, I., Noureddine, O., Gatfaoui, S., Issaoui, N., Roisnel, T., Marouani, H., 2020. Experimental, computational, and in silico analysis of (C8H14N2) 2 [CdCl6] compound. J. Mol. Struct. 128186.

Kosar, B., Albayrak, C., 2011. Spectrochim. Acta A 78, 160–167.

Lecuit, M., 2020. Chloroquine and COVID-19, where do we stand. Med. Maladies Infect. 50, 229.

Lee, C., Yang, W., Parr, R.G., 1988. Development of the Colle-Salvetti correlation-energy formula into a functional of the electron density. Phys. Rev. B 37, 785–789.

Liu, C., Zhang, D., Gao, M., Liu, S., 2015. Chem. Res. Chin. Univ. 31, 597–602.

G. M. Morris, R. Huey, J. O. Arthur, Using autodock for ligand-receptor dockingCurr Protoc Bioinformatics. 24 (2008) 8-14.

Noureddine, O., Gatfaoui, S., Brandan, S.A., Marouani, H., Issaoui, N., 2020a. Structural, docking and spectroscopic studies of a new piperazine derivative, 1-phenylpiperazine-1,4-diium-bis (hydrogen sulfate). J. Mol. Struct. 1202, 127351.

Noureddine, O., Gatfaoui, S., Brandan, S.A., Saagama, A., Marouani, H., Issaoui, N., 2020b. Experimental and DFT studies on the molecular structure, spectroscopic properties, and molecular docking of 4-phenylpiperazine-1-ium dihydrogen phosphate. J. Mol. Struct. 1207, 127762.

O'Boyle, N.M., Tenderholt, A.L., Langer, K.M., 2008. A library for package independent computational chemistry algorithms. J. Comput. Chem. 29, 839–845.

Parr, R.G., Pearson, R.G., 1983. Absolute hardness: companion parameter to absolute electronegativity. J. Am. Chem. Soc. 105, 7512–7516.

Reed, A.E., Weinhold, F., 1985. Natural localized molecular orbitals. Chem. Phys 83, 1736–1740.

Romani, D., Noureddine, O., Issaoui, N., Brandán, S.A., 2020. Properties and reactivities of niclosamide in different media, a potential antiviral to treatment of COVID-19 by using DFT calculations and molecular docking. Biointerface Res. Appl. Chem. 10, 7295–7328.

E. Romano, N. Issaoui, M. E. Manzur, S. A. Brandán, Properties and molecular docking of antiviral to COVID-19 chloroquine combining DFT calculations with SQMFF approach, Inter. J. of Current Adv. Research, Volume 9, Issue 08(A), (2020) 22862-22876.

Sagaama, A., Brandan, S.A., Ben Issa, T., Issaoui, N., 2020. Searching potential antiviral candidates for the treatment of the 2019 novel coronavirus based on DFT calculations and molecular docking. Heliyon 6, (8) e04640.

Sagaama, A., Noureddine, O., Brandán, S.A., Jarczyk-Jędryka, A., Flakus, H.T., Ghalla, H., Issaoui, N., 2020. Molecular docking studies, structural and spectroscopic properties of monomeric and dimeric species of benzofuran-carboxylic acids derivatives: DFT calculations and biological activities. Computat. Biol. Chem. 107311.

Seeliger, D., de Groot, B.L., 2010. Ligand docking and binding site analysis with PyMOL and Autodock/Vina. J. Comput. Aided Mol. Des. 24, 417–422.

Touret, F.X., 2020. Lamballerie of chloroquine and COVID-19. Antiv. Res. 104762

D.S. Visualizer, Accelrys software inc. Discovery Studio Visualizer. 2 (2005).

Wang, C., Horby, P.W., Hayden, F.G., 2020. A novel Coronavirus outbreak of global health concern. Lancet 395, 470–473.

Xavier, S., Periandy, S., 2015. Spectroscopic (FT-IR, FT-Raman, UV and NMR) investigation on 1-phenyl-2-nitropropene by quantum computational calculations. Spectrochim. Acta Part A 149, 216–230.

Yang, J.-M., Chen, C.-C., 2004. GEMDOCK: a generic evolutionary method for molecular docking Proteins. Struct. Funct. Bioinform. 55, 288–304.